



HAL
open science

Cosserat approach to localization in geomaterials

Ioannis Stefanou, Jean Sulem, Hadrien Rattiez

► **To cite this version:**

Ioannis Stefanou, Jean Sulem, Hadrien Rattiez. Cosserat approach to localization in geomaterials. 2016. hal-01471290

HAL Id: hal-01471290

<https://enpc.hal.science/hal-01471290>

Preprint submitted on 19 Feb 2017

HAL is a multi-disciplinary open access archive for the deposit and dissemination of scientific research documents, whether they are published or not. The documents may come from teaching and research institutions in France or abroad, or from public or private research centers.

L'archive ouverte pluridisciplinaire **HAL**, est destinée au dépôt et à la diffusion de documents scientifiques de niveau recherche, publiés ou non, émanant des établissements d'enseignement et de recherche français ou étrangers, des laboratoires publics ou privés.

Cosserat approach to localization in geomaterials

Ioannis Stefanou, Jean Sulem and Hadrien Rattetz

Université Paris-Est, Laboratoire Navier, CERMES, CNRS (UMR 8205), ENPC, IFSTTAR

Abstract: A renewed interest towards Cosserat or micropolar continuum has driven researchers to the development of specific constitutive models for upscaling discrete media such as masonry, granular assemblies, fault gouges, porous media and biomaterials. Cosserat continuum is a special case of what is called micromorphic, generalized or higher order continua. Due to the presence of internal lengths in its formulation, Cosserat continuum is quite attractive for addressing problems involving strain localization. It enables modeling the shear band thickness evolution, tracking the post localization regime and correctly dissipating the energy when using numerical schemes. In this chapter we summarize the fundamental governing equations of a Cosserat continuum under multiphysical couplings. Several examples of the numerical advantages of Cosserat continuum are also presented regarding softening behavior, strain localization, finite element formulation, reduced integration and hourglass control. The classically used constitutive models in Cosserat elastoplasticity are presented and some common approaches for upscaling and homogenization in Cosserat continuum are discussed. Finally, a simple illustrative example of the adiabatic shearing of a rock layer under constant shear stress is presented in order to juxtapose a rate-independent Cosserat with a rate-dependent Cauchy formulation as far as it concerns strain localization.

1. Introduction

Cosserat or micropolar continuum is a special case of what is called micromorphic, generalized or higher order continua. The general theory of micromorphic continua is general enough to represent various heterogeneous systems with microstructure. In Figure 1 we briefly outline the various higher order continuum theories according to Germain [1] and their special cases. Besides the classical continuum (also called Cauchy or Boltzmann continuum) and the Cosserat continuum, special cases of micromorphic continua are also the second gradient and the couple stress continuum theories.

In the last three decades, a renewed interest towards the Cosserat continuum has driven researchers to the development of specific continuous models for up-

scaling discrete media such as masonry, granular assemblies, fault gouges, porous media and biomaterials (see for instance [2]–[15] among others). Cosserat continuum has seemed motivated by the advantages enclosed in its enhanced kinematics and the non-symmetry of the stress tensor. When used for the formulation of continuum equivalent models for discrete media, Cosserat continuum allows to efficiently take into account high deformation gradients, relative particles' rotation and scale effects. Moreover, Cosserat continuum enables the investigation of the phenomenon of wave dispersion, which characterizes the dynamic response of discrete media when the wavelength is comparable to the size of the microstructure (internal length).

Due to the presence of internal lengths in its formulation, Cosserat continuum is quite attractive for addressing problems involving strain localization. After the pioneering work of [11] who explained mathematically the shear band thickness and its evolution under shearing, Cosserat continuum became the first and nowadays one of the common modeling approaches for regularization of the ill-posed Cauchy continuum [16]–[20]. Moreover, the correct simulation of the shear band thickness evolution (e.g. the thickness of the principal slip zone in a fault gouge) and of the post peak behavior of a system, which Cosserat theory enables, guarantees the correct energy dissipation of a system.

This chapter is structured as follows. In section 2 we give the general equations of a Cosserat continuum. In particular, the linear and angular momentum balance as well as the mass and energy balance equations and the second law of thermodynamics are extended for the Cosserat continuum. Under multiphysical couplings, involving chemistry and phase transformations, the above equations have to be adapted for momentum, mass and energy exchange between the considered phases. Section 2 is completed with a small paragraph discussing the additional terms due to this exchange. In section 3, we present some constitutive laws that are commonly used in Cosserat elasticity and elastoplasticity, including softening and multiphysical couplings. In section 4, we show the numerical advantages of Cosserat continuum theory for solving problems when softening behavior and strain localization are encountered. The commonly used approaches for upscaling and homogenization of heterogeneous structures in the frame of Cosserat continuum are discussed in section 5. Finally, in section 6, a simple example of the adiabatic shearing of a rock layer under constant shear stress is presented in order to highlight the similarities of a rate independent Cosserat and a rate dependent Cauchy continuum as far it concerns the conditions for which shear band localization takes place. It is worth mentioning that Cosserat continuum is a promising framework in fault mechanics as it enables to compute the thickness of the principal slip zone inside a fault core, its dependence upon the microstructure of the fault gouge, [8], [21]–[24] and its impact on the seismic energy budget.

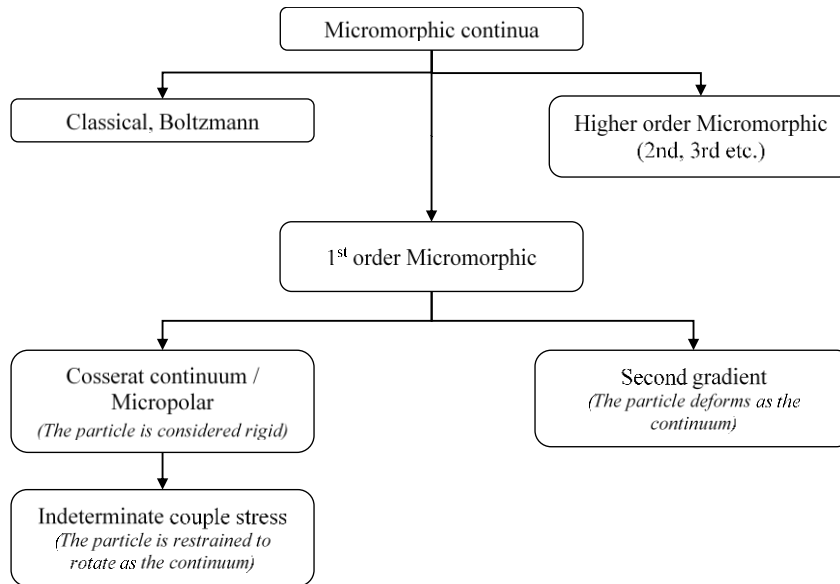


Figure 1. Higher order continuum theories according to Germain's terminology [25], [26]

2. The Cosserat continuum

Cosserat continuum equations can be derived in two different, but equivalent ways, each one based on a different physical ansatz. The first one is based on the linear and angular momentum balance and the fundamental assumption of the existence of the so-called couple stresses at the material point (Figure 2). The physical meaning of couple stresses, as well of their conjugate in energy kinematic measures, i.e. the gradient of the rotations (i.e. the curvatures), is a long-standing point of discussions in the scientific community and it is application-wise. For instance, in the Timoshenko theory of beams, which coincides with a one dimensional Cosserat continuum, the Cosserat moment is simply the resultant section moment. The physical meaning of the Cosserat moments, rotations and curvatures is debatable. However, the same holds for the stress in the classical, Cauchy continuum. All these quantities of classical and non-classical continua should rather be investigated in the frame of regular and/or singular distribution theory, which offers a greater flexibility in the modeling and measurement of physical quantities of heterogeneous media, such as geomaterials are.

The second, alternative approach for deriving the Cosserat continuum equations is by postulating the form of the energy density function and by enriching directly the kinematics of the material point. Both ways are equivalent, but here we

prefer to present the first one as only the momentum balance equations are needed. The energy of a Cosserat continuum can be then derived directly from the variational form of the Cosserat equilibrium equations.

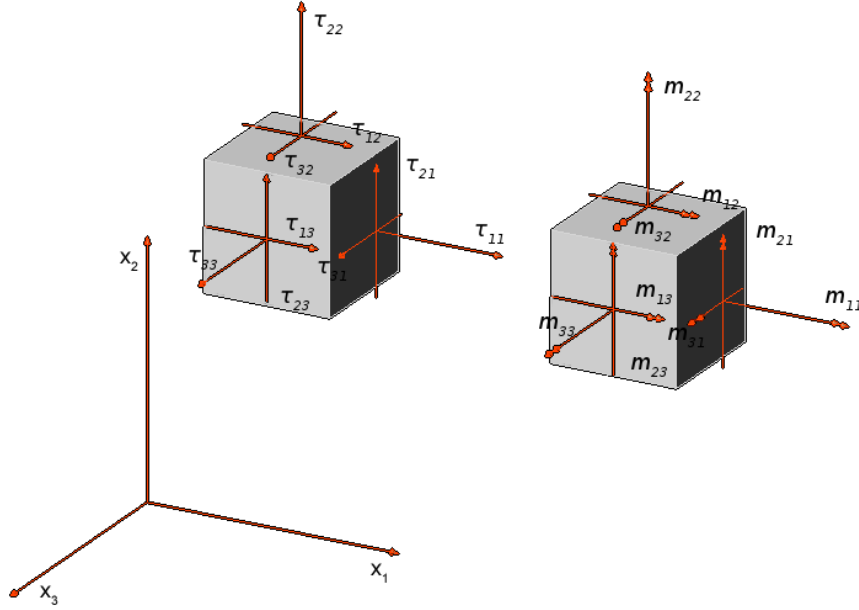


Figure 2. Stresses and couple-stresses (moments) of Cosserat continuum [27]

2.1 Linear and angular momentum balance

Let us consider a solid of volume V and its boundary ∂V . The linear momentum is given as follows:

$$P_i = \int_V \rho v_i dV \quad (1)$$

where v_i is the velocity of a material point, $i = 1, 2, 3$ (in three dimensions) and ρ is the density. The resultant force is written as:

$$F_i = \int_V f_i dV + \int_{\partial V} t_i dS \quad (2)$$

where f_i is a body force per unit volume and t_i is the traction vector, with $t_i = \tau_{ij}n_j$ and n_j the normal unit vector at the boundary. Repeated indices denote summation over the repeated index. Applying the Newton's law $\frac{DP_i}{Dt} = F_i$, we obtain:

$$\tau_{ij,j} + f_i = \rho \frac{Dv_i}{Dt} \quad (3)$$

In the case of a multi-phase material the velocity of each constituent phase has to be considered separately. Moreover, the momentum equations have to be written separately for each phase and then combined to give again Eq.(3), but with $\rho \frac{Dv_i}{Dt} = (1-n)\rho^s \frac{D^s v_i^s}{Dt} + n\rho^f \frac{D^f v_i^f}{Dt}$, where, here, f stands for the fluid phase and s for the solid one, n is the Eulerian porosity (pore volume per unit volume of porous material in actual state) and $\frac{D^x(\cdot)}{Dt} = \frac{\partial(\cdot)}{\partial t} + (\cdot)_{,i}v_i^x$. The above equation is valid as far as no exchange or transformation takes place between the phases.

The moment of momentum about a point is:

$$H_i = \int_V e_{ijk}x_j \rho v_k dV + \int_V I_{ij} \omega_j dV \quad (4)$$

where e_{ijk} is the Levi-Civita perturbation symbol, I_{ij} the microinertia tensor and ω_j the Cosserat rotational velocity of the material point. In the special case of an isotropic microinertia tensor, $I_{ij} = I_s \delta_{ij}$, where δ_{ij} is the Kronecker delta.

The resultant moment about the same point is written as:

$$L_i = \int_V (e_{ijk}x_j f_k + \mu_i) dV + \int_S e_{ijk}x_j t_k dS + \int_V m_i dS \quad (5)$$

where μ_i is a body couple stress per unit volume and $m_i = m_{ij}n_j$ is the couple stress tractor, with m_{ij} the couple stress tensor. Euler's law $\frac{DH_i}{Dt} = L_i$, yields:

$$m_{ij,j} + e_{ijk} \tau_{kj} = I_{ij} \frac{D\omega_j}{Dt} \quad (6)$$

From the above equation we observe that the stress tensor τ_{ij} is not

symmetric due to the presence of the couple stress gradient and the microinertia terms. τ_{ij} can be decomposed into a symmetric σ_{ij} and an antisymmetric part s_{ij} : $\tau_{ij} = \sigma_{ij} + s_{ij}$. In this case the symmetric part plays the role of the Cauchy stress tensor.

2.2 Mass balance

The derivation of the pore pressure diffusion generation equation from the mass balance follows the classical derivation procedure as in the classical Cauchy continuum. In particular it becomes:

$$\frac{\partial p^f}{\partial t} = \Lambda \frac{\partial T}{\partial t} - \frac{1}{\beta^*} \frac{\partial \varepsilon}{\partial t} + \frac{1}{\beta^*} w_{i,i} \quad (7)$$

where $w_i = n(v_i^f - v_i^s)$ is the Darcy's fluid (relative) velocity, $\frac{\partial \varepsilon}{\partial t} = v_{i,i}$ is the volumetric strain rate, $\Lambda = \frac{\lambda^*}{\beta^*}$ is the undrained pore fluid pressurization coefficient, with $\lambda^* = n\lambda^f + (1-n)\lambda^s$ where λ^f is the fluid thermal expansion coefficient and λ^s is the solid thermal expansion coefficient, $\beta^* = n\beta^f + (1-n)\beta^s$ is the storage coefficient, where β^f is the fluid compressibility and β^s is the compressibility of the solid phase.

Assuming Darcy's law for the fluid flow, the above equation becomes:

$$\frac{\partial p^f}{\partial t} = \Lambda \frac{\partial T}{\partial t} - \frac{1}{\beta^*} \frac{\partial \varepsilon}{\partial t} + c_{hy} p_{,ii}^f \quad (8)$$

where $c_{hy} = \frac{k}{\eta_f \beta^*}$ is the hydraulic diffusivity with k the hydraulic permeability, which is assumed here isotropic and constant and η_f the fluid viscosity.

2.3 Energy balance

Similarly to the mass balance equation, the derivation of the energy balance equation and in a second step of the heat equation follows the same steps as in the

case of the Cauchy continuum. However, the work of the external, generalized forces and the kinetic energy have some additional terms due to the Cosserat rotations and moments. More specifically, assuming a micropolar solid phase and a non-micropolar fluid the kinetic energy rate is:

$$\begin{aligned} \frac{DK}{Dt} &= \frac{DK^s}{Dt} + \frac{DK^f}{Dt} \\ &= \frac{D}{Dt} \left\{ \int_V \left[\frac{1}{2} (1-n) \rho^s v_i^s v_i^s + \frac{1}{2} (1-n) I^s \omega_i \omega_i \right] dV \right. \\ &\quad \left. + \int_V \frac{1}{2} n \rho^f v_i^f v_i^f dV \right\} \end{aligned} \quad (9)$$

The internal energy is written as follows:

$$\begin{aligned} \frac{DE}{Dt} &= \frac{DE^s}{Dt} + \frac{DE^f}{Dt} \\ &= \frac{D}{Dt} \int_V \left[(1-n) \rho^s \mathcal{E}^s + n \rho^f \mathcal{E}^f \right] dV \end{aligned} \quad (10)$$

where \mathcal{E}^s and \mathcal{E}^f are the internal energy of the solid and fluid phase respectively per unit mass.

The work rate of external forces for a Cosserat continuum is given by:

$$\frac{DW}{Dt} = \int_{\partial V} (t_i^s v_i^s + m_i \omega_i + t_i^f v_i^f) dS + \int_V (f_i^s v_i^s + \mu_i \omega_i + f_i^f v_i^f) dV \quad (11)$$

Notice that due to the presence of two phases in the medium the volumetric as well as the external generalized forces and tractions are split over the two phases. For a chemically inert system and in absence of any exchange between the solid and the fluid phase the equations remain the same with (3) and (6). According to the first law of thermodynamics we have:

$$\frac{DK}{Dt} + \frac{DE}{Dt} = \frac{DQ}{Dt} + \frac{DW}{Dt} \quad (12)$$

where $\frac{DQ}{Dt} = - \int_{\partial V} h_i n_i dS = - \int_V h_{i,i} dV$ is the rate of heat input (given to V through its boundary ∂V) and h_i is the heat flux vector components. After some algebraic manipulations, the energy balance equation becomes:

$$\begin{aligned}
& (1-n)\rho^s \frac{D^s \mathcal{E}^s}{Dt} + n\rho^f \frac{D^f \mathcal{E}^f}{Dt} + \rho^f \mathcal{E}_{,i}^f w_i \\
& - \tau_{ij} \dot{\gamma}_{ij} - m_{ij} \dot{\kappa}_{ij} + h_{i,i} \\
& + (p^f w_i)_{,i} - \rho^f \left(f_i - \frac{D^f v_i^f}{Dt} \right) w_i = 0
\end{aligned} \tag{13}$$

where $\dot{\gamma}_{ij} = v_{i,j} + e_{ijk} \omega_k$ and $\dot{\kappa}_{ij} = \omega_{i,j}$. Neglecting the Cosserat effects, the above equation coincides with [28], [29].

Assuming an elastoplastic constitutive law (see section 3) the energy balance equation results to the heat equation for Cosserat continua:

$$\frac{\partial T}{\partial t} = c_{th} \frac{\partial^2 T}{\partial x_i \partial x_i} + \frac{1}{\rho C} \tau_{ij} \dot{\gamma}_{ij}^p + \frac{1}{\rho C} m_{ij} \dot{\kappa}_{ij}^p \tag{14}$$

where, T is the temperature, $\dot{\gamma}_{ij}^p$ the plastic deformation rate tensor and $\dot{\kappa}_{ij}^p$ the plastic curvature rate tensor and c_{th} the thermal diffusivity coefficient. For deriving the above equation, small deformations and an isotropic Fourier's law were considered.

2.4 Second law of thermodynamics

Following the same derivations the second law of thermodynamics yields:

$$\int_V \left[\frac{D^s S}{Dt} - (S - S^f)(\rho^f w_i)_{,i} + S_{,i}^f \rho^f w_i + \left(\frac{h_i}{T} \right)_{,i} \right] dV \geq 0 \tag{15}$$

where S denotes the specific entropy of the mixture per unit mass and S^x the specific entropy of the specie x . The above equation coincides with the one of [28] after proper substitutions and algebra. Under specific assumptions for the constitutive behavior of the solid and the fluid phases the above equation can be further developed.

2.5 Phase transitions between the species

Phase transitions from the solid to the fluid phase and vice versa due to, for instance, dissolution/precipitation mechanisms or dehydration, has as a result the

addition of supplementary terms in the above equations. In particular, if $\dot{r}_{s \rightarrow f} = -\dot{r}_{f \rightarrow s}$ expresses the rate of transition from the solid to the fluid phase, equations (3), (6), (8), (13) and (15) become:

$$\tau_{ij,j} + f_i + (v_i^f - v_i^s)\dot{r}_{s \rightarrow f} = \rho \frac{Dv_i}{Dt} \quad (16)$$

$$m_{ij,j} + e_{ijk}\tau_{kj} + \alpha\omega_i\dot{r}_{s \rightarrow f} = I_{ij} \frac{D\omega_j}{Dt} \quad (17)$$

$$\frac{\partial p^f}{\partial t} = \Lambda \frac{\partial T}{\partial t} - \frac{1}{\beta^*} \frac{\partial \varepsilon}{\partial t} + \frac{1}{\beta^*} w_{i,i} - c_{ch}\dot{r}_{s \rightarrow f} \quad (18)$$

$$\begin{aligned} & (1-n)\rho^s \frac{D^s \mathcal{E}^s}{Dt} + n\rho^f \frac{D^f \mathcal{E}^f}{Dt} + \rho^f \mathcal{E}_{,i}^f w_i \\ & - \tau_{ij}\dot{\gamma}_{ij} - m_{ij}\dot{\kappa}_{ij} + h_{i,i} \\ & + (p^f w_i)_{,i} - \rho^f \left(f_i - \frac{D^f v_i^f}{Dt} \right) w_i \\ & + \dot{r}_{s \rightarrow f} \frac{1}{2} \left[(v_i^f - v_i^s)(v_i^f - v_i^s) + \alpha\omega_i\omega_i + 2(\mathcal{E}^f - \mathcal{E}^s) \right] = 0 \end{aligned} \quad (19)$$

$$\begin{aligned} & \int_V \left[\frac{D^s S}{Dt} - (S - S^f)(\rho^f w_i)_{,i} + S_{,i}^f \rho^f w_i + \left(\frac{h_i}{T} \right)_{,i} \right] dV \\ & + \int_V \dot{r}_{s \rightarrow f} (S^f - S^s) dV \geq 0 \end{aligned} \quad (20)$$

where $c_{ch} = \frac{1}{\beta^*} \frac{\rho^f - \rho^s}{\rho^f \rho^s}$ is the chemical pressurization coefficient and $\alpha = \frac{I_s}{\rho_s}$.

The chemical pressurization coefficient may be insignificant in most of the cases of dissolution/precipitation reactions in rocks [30]. However, this is not the case for dehydration or decarbonation reactions [31], [32].

3. Constitutive laws for Cosserat continua

Deriving constitutive relations for Cosserat continuum is not a trivial task. This is owed to the fact that Cosserat theory has intrinsic internal lengths and consequently the constitutive law is not scale invariant. In the simplest case, i.e. under

small deformations, in a centrosymmetric, linear, elastic, isotropic Cosserat medium, the stresses are related to the generalized elastic deformation measures according to the following constitutive relations [33]:

$$\begin{aligned}\tau_{ij} &= K\gamma_{kk}^{el}\delta_{ij} + 2G\left(\gamma_{(ij)}^{el} - \frac{1}{3}\gamma_{kk}^{el}\delta_{ij}\right) + 2\eta_1 G\gamma_{[ij]}^{el} \\ m_{ij} &= 4GR^2\left(\kappa_{(ij)}^{el} + \eta_2\delta_{ij}\kappa_{kk}^{el}\right) + 4GR^2\eta_3\kappa_{[ij]}^{el}\end{aligned}\quad (21)$$

where K is the bulk modulus, G is the shear modulus, η_1 , η_2 , η_3 are positive material constants and R is an internal length parameter, which for granular materials is often identified to the mean radius of the grains in the Representative Volume Element (RVE). $\gamma_{(ij)}$ and $\gamma_{[ij]}$ denote respectively the symmetric and anti-symmetric parts of $\gamma_{ij} = u_{i,j} + e_{ijk}\theta_k$, where u_i are the components of the displacement vector and θ_k the components of the Cosserat rotation vector (infinitesimal rotations). The Cosserat shear modulus, which expresses the stiffness related to the relative rotation of the particle (e.g. of a grain) with respect to the macro-rotation of the continuum (e.g. assemblage of grains) is defined as $G_c = \eta_1 G$.

	2D model	3D model
Static consideration	$h_i = \{\frac{3}{4}, \frac{-1}{4}, 1, 0\}$ $g_i = \{\frac{3}{2}, \frac{1}{2}, 1, 0\}$	$h_i = \{\frac{2}{3}, \frac{-1}{6}, \frac{2}{3}, \frac{-1}{6}\}$ $g_i = \{\frac{8}{5}, \frac{2}{5}, \frac{8}{5}, \frac{2}{5}\}$
Kinematical consideration	$h_i = \{\frac{3}{8}, \frac{1}{8}, \frac{1}{4}, 0\}$ $g_i = \{3, -1, 4, 0\}$	$h_i = \{\frac{2}{5}, \frac{1}{10}, \frac{2}{5}, \frac{1}{10}\}$ $g_i = \{\frac{8}{3}, \frac{-2}{3}, \frac{8}{3}, \frac{-2}{3}\}$

Table 1. Coefficients used for the generalized J2 invariants for Cosserat continuum [34]

In a small deformations framework the classical J2 plasticity criteria can be generalized for Cosserat continua. This approach is based on the generalization of the stress and strain invariants in order to account for the Cosserat couple stresses, curvatures and rotations. Based on micromechanical considerations and averaging, the deviatoric stress and strain invariants take the following form [22], [35], [36]:

$$\begin{aligned}q &= \sqrt{h_1 \tau_{ij}^d \tau_{ij}^d + h_2 \tau_{ij}^d \tau_{ji}^d + \frac{1}{R^2} (h_3 m_{ij}^d m_{ij}^d + h_4 m_{ij}^d m_{ji}^d)} \\ \gamma &= \sqrt{g_1 \gamma_{ij}^d \gamma_{ij}^d + g_2 \gamma_{ij}^d \gamma_{ji}^d + R^2 (g_3 \kappa_{ij}^d \kappa_{ij}^d + g_4 \kappa_{ij}^d \kappa_{ji}^d)}\end{aligned}\quad (22)$$

where τ_{ij}^d , m_{ij}^d , γ_{ij}^d and κ_{ij}^d are the deviatoric parts of the stress, couple-stress, strain and curvature tensors respectively. h_p and g_p ($p=1,\dots,4$) are coefficients that can be determined by micro-mechanical considerations on the kinematics or the statics of an assemblage of grains in contact [34], [37] (see Table 1).

Notice that the internal length R appears directly in the above expressions. Once the above invariants are derived, various plasticity criteria can be used. We refer for example to the von Mises, the Drucker-Prager or to the Cam-clay criterion, which are commonly used in metal, soil and rock mechanics and they are expressed in terms of the q, p invariants. Volumetric and shear hardening parameters can be also defined allowing not only to reproduce the stress-strain response of a geomaterial, but also the shear band thickness evolution [38], its thickness and the post-bifurcation regime, which is crucial in many applications as it is related to stress redistribution, collapse and energy dissipation. In a small strains framework the generalized deformation measures are decomposed in elastic and plastic parts as follows:

$$\begin{aligned}\dot{\gamma}_{ij} &= \dot{\gamma}_{ij}^{el} + \dot{\gamma}_{ij}^{pl} \\ \dot{\kappa}_{ij} &= \dot{\kappa}_{ij}^{el} + \dot{\kappa}_{ij}^{pl}\end{aligned}\quad (23)$$

Assuming a Drucker-Prager yield surface and plastic potential:

$$F = q + \mu p \leq 0 \quad (24)$$

:

$$Q = q + \beta p \quad (25)$$

where $p = \tau_{kk}$, μ is the friction coefficient and β the dilatancy coefficient, the elasto-plastic incremental generalized stress-strain relationships become:

$$\begin{aligned}\dot{\tau}_{ij} &= C_{ijkl}^{ep} \dot{\gamma}_{kl} + D_{ijkl}^{ep} \dot{\kappa}_{kl} + E_{ijkl}^{ep} \dot{T} \delta_{kl} \\ \dot{\mu}_{ij} &= M_{ijkl}^{ep} \dot{\kappa}_{kl} + L_{ijkl}^{ep} \dot{\gamma}_{kl} + N_{ijkl}^{ep} \dot{T} \delta_{kl}\end{aligned}\quad (26)$$

where:

$$\begin{aligned}
C_{ijkl}^{ep} &= C_{ijkl}^e - \frac{\langle 1 \rangle}{H_p} b_{ij}^Q b_{kl}^F & D_{ijkl}^{ep} &= -\frac{\langle 1 \rangle}{H_p} b_{ij}^Q b_{kl}^{FM} \\
E_{ijkl}^{ep} &= -(C_{ijkl}^e - \frac{\langle 1 \rangle}{H_p} b_{ij}^Q b_{kl}^F) & L_{ijkl}^{ep} &= -\frac{\langle 1 \rangle}{H_p} b_{ij}^Q b_{kl}^F \\
M_{ijkl}^{ep} &= M_{ijkl}^e - \frac{\langle 1 \rangle}{H_p} b_{ij}^Q b_{kl}^{FM} & N_{ijkl}^{ep} &= \frac{\langle 1 \rangle}{H_p} b_{ij}^Q b_{kl}^F
\end{aligned} \tag{27}$$

C_{ijkl}^e and M_{ijkl}^e are the elastic constitutive tensors for the stress and the couple stress respectively, derived from Eq. (21), and

$$\begin{aligned}
b_{kl}^F &= \frac{\partial F}{\partial \tau_{ij}} C_{ijkl}^e; & b_{ij}^Q &= C_{ijkl}^e \frac{\partial F}{\partial \tau_{kl}}; & b_{kl}^{FM} &= \frac{\partial F}{\partial \mu_{ij}} M_{ijkl}^e \\
H_p &= \frac{\partial F}{\partial \tau_{ij}} C_{ijkl}^e \frac{\partial Q}{\partial \tau_{kl}} + \frac{\partial F}{\partial \mu_{ij}} M_{ijkl}^e \frac{\partial Q}{\partial \mu_{kl}} + H_s
\end{aligned} \tag{28}$$

H_s is the hardening modulus due to shear plastic deformations, defined by:

$$\frac{\partial F}{\partial \gamma^p} = -H_s \tag{29}$$

Once the constitutive parameters of the material are calibrated, a bifurcation analysis can provide important information regarding strain localization evolution under shearing [38]. Various multiphysical phenomena [8], [23], [39] as well as grain cataclasis [22] can also be considered. Predicting strain localization is of paramount importance in geotechnical applications involving strongly non-associated materials (common case) and in fault mechanics where the mutiphysical couplings, energy dissipation, softening behavior and grain size evolution play the central role for earthquake triggering and co-seismic slip (see next sections for more details).

It is worth emphasizing that the internal length(s) that are present in the Cosserat continuum theory have somehow to be determined or identified. This can be done either by using bottom-up, upscaling and homogenization techniques that consider the microstructure in detail (see section 5) or through classical geotechnical tests. However, in practice of classical geotechnical testing the calibration of these parameters is ignored.

4. Numerical advantages of Cosserat continuum

4.1 Mesh dependency and its remedy

It is well known that when it comes to strain localization the governing equation based on a classical, Boltzmann continuum become ill-posed and when numerical approaches are used for integration of these equations the result is mesh dependency (e.g. [40]). With the term mesh dependency we mean that the numerical results depend on the size and the type of the finite elements used. More specifically, the global behavior depends on the choice of the mesh and by refining it no convergence of the numerical results is observed. In Figure 3 we present this mathematical and numerical artifact, which is owed to the absence of internal lengths in the classical continuum. Moreover, the developed shear bands (contracting or dilating) are always 1-2 finite elements thick.

Cosserat continuum is one of the available techniques for regularizing mesh dependency during shear banding [19], [40], [41]. In Figure 4 we present the simulations that were carried out using COSS8R finite element, a homemade User Element for Abaqus, which is currently extended for use to any classical Finite Element code [20]. The problem treated is a thin hollow cylinder made of a softening material under shearing. Three different finite element discretizations were tested. In the same figure we present the resulting macroscopic behavior of the cylinder in terms of the normalized reaction moment and the differential axial rotation. The onset of plastic deformations rapidly culminates with a softening branch, which is accompanied by strain localization.

Strain localization occurs exactly as in the shear layers studied by [42]. The curves show important mesh-independency, i.e. the thickness (width) of the localization zone does not depend on the number of elements falling inside this zone and the total force-axial rotation curve is independent of the mesh size. This is a fundamental feature of finite elements based on the Cosserat continuum, but also it demonstrates the fast convergence of the chosen Finite Element interpolation scheme [43].

Besides failure analysis in geotechnical engineering [44], the post peak behavior of the geomaterial plays a crucial role in earthquake nucleation. In the idealistic, basic case of considering a fault zone as an interface with no multiphysical couplings and assuming a rate independent behaviour for the rock material, i.e. $F = F(\delta)$, where F is the interface friction and δ the slip (Figure 5 left), bifurcation theory leads (see [45], [46]) to the classical relationship for earthquake nucleation: $dF(\delta)/d\delta \leq -k$ [47]. This condition is presented graphically in Figure 5 (right). Instabilities are triggered (or induced) not at the peak, but in the softening branch, i.e. at B-C. Before that, there is slip but it is *aseismic*. This shows the importance of correctly capturing the post peak behavior of the rock material (numerically and analytically). Moreover, correct simulation of the shear band thick-

ness evolution (e.g. the thickness of the principal slip zone in a fault) guarantees that the dissipation of energy through the various multiphysical mechanisms that take place (e.g. temperature and pore pressure increase, shear heating, thermal pressurization, thermally induced chemical reactions, grain size evolution etc.) is correctly calculated before and during the seismic slip.

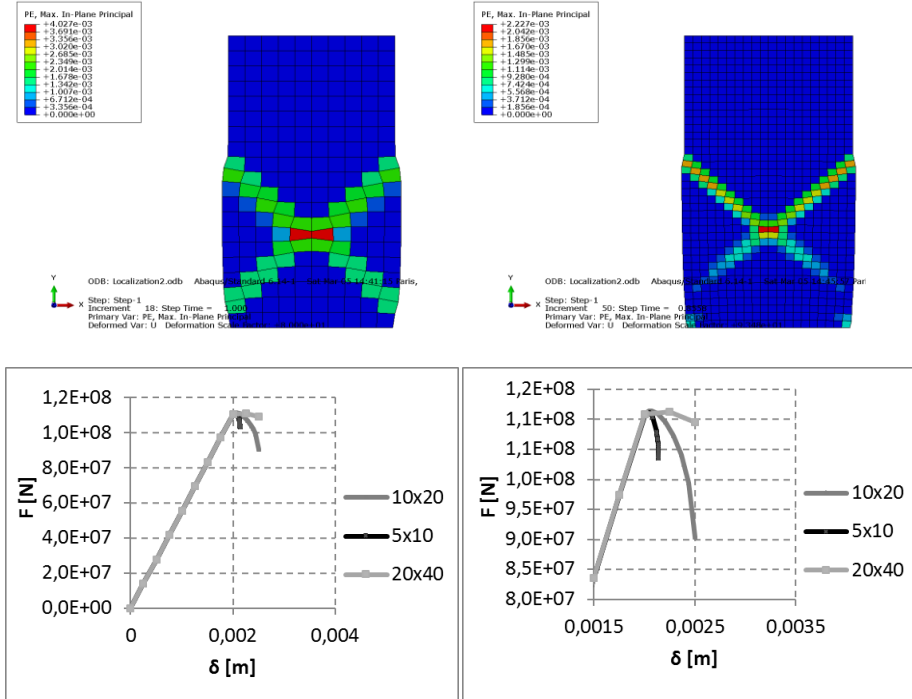
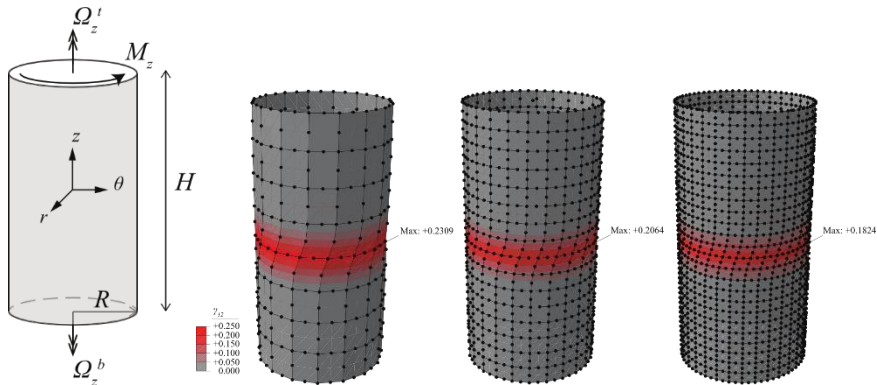


Figure 3. Biaxial test of a softening material for different mesh sizes. The developed plastic deformations, the shear band thickness and the total applied force – displacement depends on the mesh size.



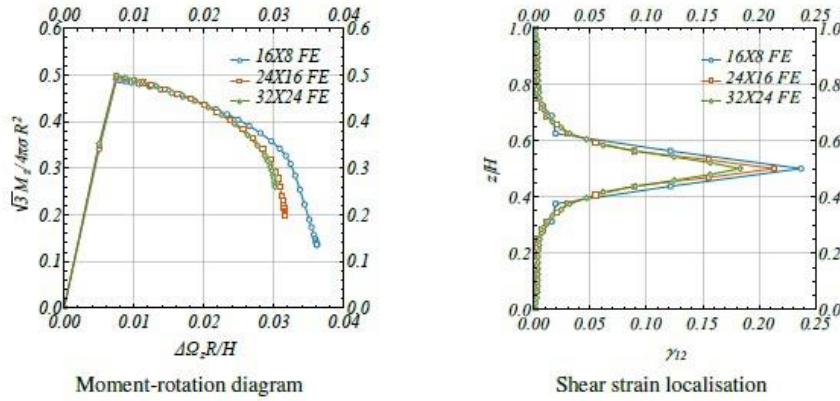


Figure 4. Above: deformation pattern and isocontour of in-plane shear strain distribution for different discretizations of the hollow cylinder. Below: Macroscopic behavior of the hollow cylinder (left) and localization of the in-plane shear strain (right) for different discretizations with the COSS8R finite element (FE) [43]

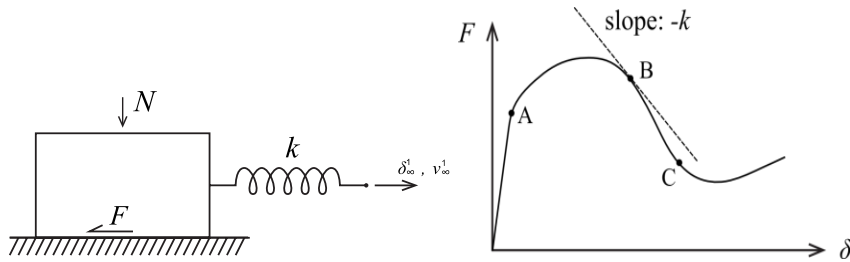


Figure 5. Left: The classical spring-slider model used for understanding earthquake nucleation and energy partition [47], [48]. Right: Schematic representation of the mechanical behavior of a rock interface (fault). From A to B the slip is aseismic. Instability takes place at B (co-seismic slip). The role of the softening branch is apparent

4.2 Shear locking, reduced integration and physical hourglass control

In the above paragraph we described the advantages of Cosserat continuum for inelastic behavior and strain localization compared to the classical continuum. Yet, Cosserat continuum numerical advantages do not stop there.

Shear locking is a common numerical problem when lower order interpolation functions are used in Finite Element analysis. Shear locking is the phenomenon of

extremely slow convergence of the numerical solution to the exact one, even when extremely fine discretizations are used. Due to the chosen interpolation functions a large ratio of the energy input is erroneously transformed to shear strain energy instead of flexural [49] resulting to a stiffer response. A numerical trick that it is commonly used in finite elements is reduced integration of the stiffness matrix. This alleviates shear locking without losing accuracy (in an incremental formulation the right-hand-side is completely/correctly integrated). However, this numerical trick comes with a price. Reduced integration of common Cauchy continuum finite elements (e.g. linear or quadratic polynomial interpolations) leads to a deficiency of the stiffness matrix. In other words, the stiffness matrix has some eigenvalues that are zero and consequently some deformation modes are associated to zero strain energy (spurious modes). For linear and quadratic Cauchy finite elements, these zero-energy modes have the geometrical shape of an hourglass. In traditional finite element technology a small artificial/numerical stiffness is added to these deformation modes (represented by the corresponding to the zero eigenvalues eigenvectors). This technique is called hourglass control. However, when important stress gradients take place, hourglass control can fail.

Cosserat continuum offers a natural way to avoid hourglass control. It can be shown [43] that after reduced integration of the stiffness matrix, no zero eigenvalues appear in the stiffness matrix. In Figure 6 we consider the well-discussed plane foundation problem [50]. Due to reduced integration, an hourglass mode is activated in the rigid element on top as a result of the applied force. This hourglass mode is able to propagate within a certain area in the elements below. On the contrary, the COSS8R element does not have this deficiency, as the rotational DOF perform an intrinsic action of hourglass control and no artificial hourglass control is needed.

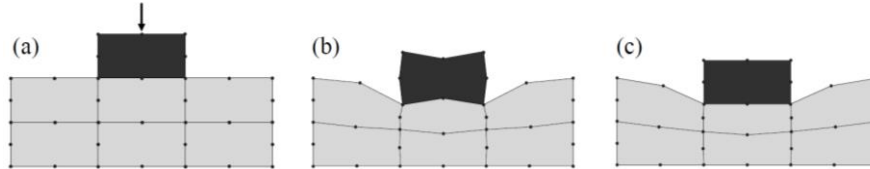


Figure 6. Foundation of a rigid footing: (a) a highly rigid element resting upon a layer of flexible elements with reduced integration; (b) propagating zero-energy mode in an assembly of Cauchy (S8R) elements; (c) accurate results from a COSS8R subdivision [43]

5. Upscaling and homogenization

Homogenization or upscaling methods is a class of methods that aim at deriving an equivalent continuum theory that describes the macroscopic behavior of

heterogeneous systems, i.e. of systems with microstructure. (Asymptotic) Homogenization is a mathematically rigorous, well established theory for performing this task [51]–[54]. This method is based on the asymptotic expansion of the various state fields (displacements, deformations, stresses) in terms of a small quantity ε , which represents the ratio of the characteristic size of the elementary volume over the overall size of the structure, and provides an equivalent to the heterogeneous system homogeneous continuum for $\varepsilon \rightarrow 0$. Besides the rigorous mathematical formulation of this approach, its main advantage is the ability to determine error estimators of the derived continuum for finite values of ε . However, when it comes to generalized continua, such as the Cosserat continuum, that possess internal lengths, the asymptotic limit $\varepsilon \rightarrow 0$ loses interest as it cancels out these internal length [55]. In other words, by this pass to the limit, asymptotic homogenization erases any internal length that are related to the material’s micro-structure, which higher order continuum theories, such as Cosserat are in principle able to capture.

To overcome this problem several alternative schemes have been proposed in the literature for upscaling heterogeneous systems (see [3], [5], [7], [9], [12], [27], [55]–[61] among others). The majority of these schemes is based upon the homogeneous equivalent continuum concept [54], in the sense that the derived Cosserat continuum shares a) the same energy (internal energy, dissipation) and b) the same kinematics with the heterogeneous, discrete medium. The classical asymptotic homogenization expansion ansatz that leads to a Cauchy continuum as the ratio of the size of the unit cell over the overall structure tends to zero is not followed in these approaches. Therefore, these heuristic approaches remain applicable even when the size of the microstructure is not infinitesimal as compared to the overall size of the system, or in other words when scale-separation is no more applicable.

A typical example for applying and testing these upscaling methods is masonry like structures. Masonry can be seen as a geomaterial whose building blocks are often quasi-periodically arranged in space. Moreover, the building blocks are at the human scale, which makes them an ideal toy-model, contrary to granular media whose microstructure is small and shows geometric complexity and has to be statistically described [62], [63]. When the upscaling scheme is correctly formulated, it is possible to capture the wave dispersion behavior of a heterogeneous system even when the wave length is comparable to the block size. Notice that in this case the classical homogeneous Cauchy continuum approach fails as it is not a dispersive medium. In Figure 7 we present the modal frequencies of a masonry panel which was upscaled with Cosserat continuum [27], [43] versus the number of its building blocks. Even when the number of the building blocks is small the Cosserat homogenized continuum model succeeds in representing the dynamics of the discrete heterogeneous structure. In Figure 8 we present the out-of-plane-displacement contours of the first three flexural modal shapes of a homogenized masonry panel and a comparison with the flexural modal shapes provided by Discrete Elements [64].

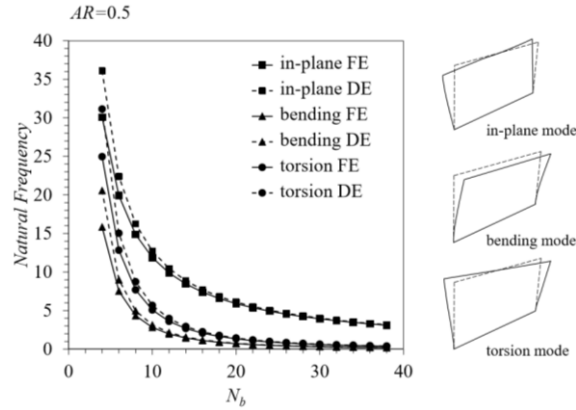


Figure 7. Modal frequencies of a masonry panel versus the number of building blocks: comparison between the results extracted by Discrete Element Method and by the use of the Cosserat homogenized plate model for masonry [20], [27]

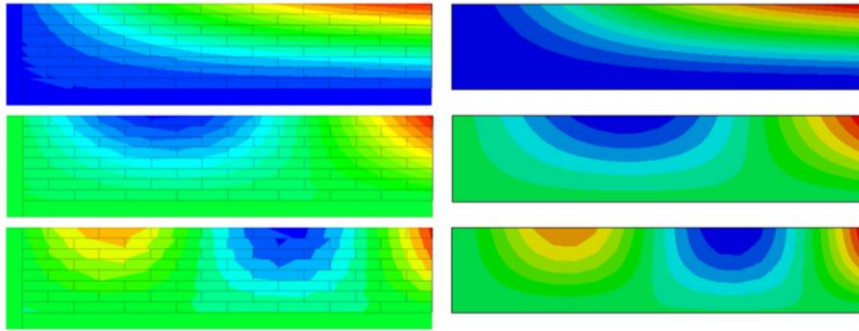


Figure 8. Out-of-plane-displacement contours of the first three flexural modal shapes. Left: Discrete Elements solution. Right: homogenized Cosserat Finite Element solution [64]

In the case of granular media the approach described in [12], [65] or in [57] can be followed for upscaling and determining the effective parameters of an equivalent Cosserat continuum. It is worth pointing that these upscaling techniques may provide valuable information on strain localization and energy dissipation in the absence of detailed experimental data as it is the case of the complex behavior of fault gouges. However, Cosserat continuum is effective under shearing. In the case of pronounced extension or compaction, the Cosserat additional terms have no effect and at least a first order micromorphic continuum has to be used (Figure 1).

6. Rock shear layer of Cosserat continuum: fault mechanics

In this section we give a simple example of Cosserat theory used for modeling the adiabatic shearing of a rock layer under constant shear stress. Two different modeling frameworks of at least, at first approximation, different physical assumptions, are juxtaposed and compared as far it concerns the conditions for which shear band localization takes place.

The first framework is the Cauchy continuum with rate-dependent constitutive law (viscoplasticity). Rate dependent constitutive models and, in general, viscoplastic constitutive laws in the frame of Cauchy continuum are frequently used as under some conditions they can lead to finite thickness shear band formation. The relation between viscosity and shear band thickness (and consequently material length scale) has been discussed in several publications (e.g. [66]). The second modeling framework is Cosserat elastoplasticity.

Thermal softening is taken into account as a destabilizing mechanism that may lead to shear band localization. The complexity of the chosen constitutive laws and of the multiphysical couplings considered is kept to a minimum degree in order to reveal the salient features of each framework and highlight their similarities and their differences as far as strain localization is concerned. For a more detailed modeling in the frame of Cosserat continuum involving thermo-poro-chemo-mechanical couplings and more elaborate constitutive laws for the rock material, the reader is referred to [8], [20], [23], [39]. The reader is referred to [67] for the Cauchy rate dependent framework under thermo-poro-chemo-mechanical couplings.

The thickness of the rock layer is D and constant normal and shear stresses are applied at its boundaries as depicted in Figure 9. Initially, the layer is considered to be in a state of homogeneous shear deformation.

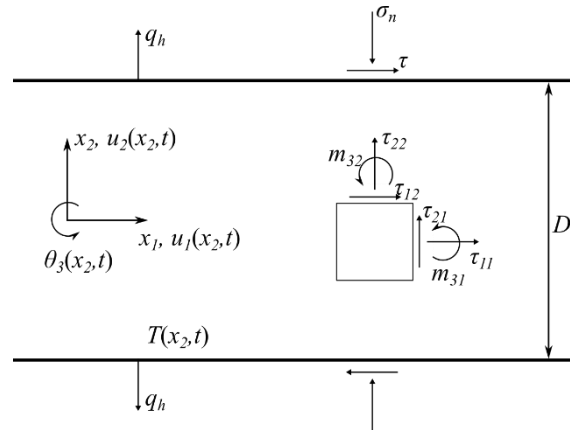


Figure 9. Shearing of a rock layer: Cosserat rotational degree of freedom ω and couple stresses

In both models it is assumed that all the plastic work is converted to heat and that Fourier's law is applicable. Under these assumptions, the heat equation is written in indicial notation as follows (see Eq.(14)):

$$\frac{\partial T}{\partial t} = c_{th} \frac{\partial^2 T}{\partial x_2^2} + \frac{1}{\rho C} \tau_{ij} \dot{\gamma}_{ij}^p + \frac{1}{\rho C} m_{ij} \dot{\kappa}_{ij}^p \quad (30)$$

where the infinite layer hypothesis was considered and consequently the derivatives in the x_1 and x_3 directions vanish (invariance). Small deformations are considered and the slip event is sufficiently rapid in order to justify adiabatic conditions at the boundaries of the layer. In the case of the Cauchy continuum the third term in the right hand side vanishes and the stress tensor is symmetric.

6.1 Cauchy continuum with rate dependent constitutive law

Let's assume a simple rate dependent constitutive law for the shear stress at a point inside the shear layer:

$$\sigma_{12} = \tau_0 + H \dot{\gamma}_{12} + \xi (T - T_s) \quad (31)$$

where H is a mechanical hardening parameter (positive), ξ a thermal softening parameter (negative), T_s a reference temperature and τ_0 the shear stress at steady state and reference temperature.

For a Cauchy continuum the linear momentum balance is:

$$\sigma_{ij,j} = 0 \quad (32)$$

Inertia terms and body forces are neglected in this example. The angular momentum balance imposes the symmetry of the stress tensor, $\sigma_{ij} = \sigma_{ji}$. For a Cauchy continuum, $\gamma_{ij} = u_{i,j}$, where u_i is the displacement in the i^{th} direction.

At steady state $T = T^* = T_s$, $\sigma_{12} = \sigma_{12}^* = \tau_0$, $\sigma_{22} = \sigma_{22}^* = \sigma_0$, $\dot{\gamma}_{12} = \dot{\gamma}_{12}^* = 0$ and $\dot{T}^* = 0$. This state will be stable as long as any perturbation does not grow in time. By perturbing the temperature and displacements fields at steady state, $T = T^* + \tilde{T}$ $u_i = u_i^* + \tilde{u}_i$) and by neglecting higher order terms, Eqs. (30), (31) and (32) become:

$$\begin{aligned}
\tilde{\sigma}_{12} &= H \dot{\gamma}_{12}^p + \xi \tilde{T}; & \frac{\partial \tilde{\sigma}_{12}}{\partial x_2} &= 0; & \frac{\partial \tilde{\sigma}_{22}}{\partial x_2} &= 0 \\
\frac{\partial \tilde{T}}{\partial t} &= c_{th} \frac{\partial^2 \tilde{T}}{\partial x_2^2} + \frac{1}{\rho C} \sigma_{12}^* \dot{\gamma}_{12}^p
\end{aligned} \tag{33}$$

The perturbations \tilde{T} , \tilde{u}_i should fulfill the boundary conditions of the rock layer. Equations (33) together with the boundary conditions $\left. \frac{\partial \tilde{T}}{\partial z} \right|_{z=\pm \frac{D}{2}} = 0$,

$\tilde{\sigma}_{12}\left(z = \pm \frac{D}{2}\right) = 0$ and $\tilde{\sigma}_{22}\left(z = \pm \frac{D}{2}\right) = 0$ form a linear system of partial differential equations which admits solutions of the type $\tilde{u}_i = U_i e^{st} \sin \frac{2\pi}{\lambda} z$, $\tilde{T} = T e^{st} \cos \frac{2\pi}{\lambda} z$, where s is the so-called growth coefficient and $\lambda = \frac{D}{N}$,

$N = 1, 2, 3, \dots$. By replacing into (33) we obtain: $s = -\frac{\xi \tau_0}{H \rho C} - \frac{4\pi^2 c_{th}}{\lambda^2}$. The system is unstable when $s > 0$ or, equivalently, when the wavelength of the perturbation is bigger than a critical wavelength λ_{cr}^{rd} : $\lambda > \lambda_{cr}^{rd} = 2\pi \sqrt{\frac{H c_{th} \rho C}{-\xi \tau_0}}$.

6.2 Cosserat elastoplasticity

An elastic perfectly plastic constitutive behavior with thermal softening is assumed in this example. More advanced Cosserat constitutive models such as the Mühlhaus-Vardoulakis Cosserat plasticity model [36] might be used (see section 3), but the advantage of this simple model is that analytical derivations are simple to perform, which permits a convenient comparison with the above rate dependent model. By analogy with the Cauchy rate dependent model presented in the previous paragraph, the yield surface is defined as:

$$F = \tau_{(12)} - \tau_0 - \xi(T - T_s) \leq 0 \tag{34}$$

where $\tau_{(ij)}$ denotes the symmetric part of the stress tensor. In this way the same shear stress limit and thermal softening with the Cauchy model is retrieved if one neglects the rate dependent term in Eq.(31). Nevertheless, because of the chosen yield surface (Eq.(34)) the plastic curvatures are zero and therefore they do not

contribute to the heat equation (Eq.(30)). A centrosymmetric, linear elastic isotropic Cosserat medium is considered (see Eq.(21)).

At steady state we have a Cauchy continuum under homogeneous shear. In particular, $\dot{T}^* = 0$, $T = T^* = T_s$, $\tau_{(12)} = \tau_{(12)}^* = \tau_0$, $\tau_{[12]} = \tau_{[12]}^* = 0$, $m_{32} = m_{32}^* = 0$ and $\sigma_{22} = \sigma_{22}^* = \sigma_0$. This state will be stable as long as any perturbation does not grow in time. The temperature, the displacement and the rotation fields at steady state are perturbed ($T = T^* + \tilde{T}$, $u_i = u_i^* + \tilde{u}_i$, $\theta_3 = \theta_3^* + \tilde{\theta}_3$) as in the Cauchy case. The perturbations \tilde{T} , \tilde{u}_i and $\tilde{\theta}_3$ have to fulfill the boundary conditions of the rock layer as in the Cauchy continuum case and additionally $\tilde{m}_{32} \left(z = \pm \frac{D}{2} \right) = 0$. A linear system is then formed which admits solutions of the form: $\tilde{u}_i = U_i e^{st} \sin \frac{2\pi}{\lambda} z$,

$\tilde{\theta}_3 = \Theta_3 e^{st} \cos \frac{2\pi}{\lambda} z$, $\tilde{T} = T e^{st} \cos \frac{2\pi}{\lambda} z$. The critical growth coefficient is then:

$$s = - \frac{16G\pi^4 R^2 \rho C c_h}{\lambda^2 \left(4G\pi^2 R^2 \rho C + (8\pi^2 R^2 + \lambda^2) \xi \tau_0 \right)}$$

where we set $G_c = G$ for simplicity.

The system is unstable when $s > 0$ or, equivalently when the wavelength of the perturbation is bigger than a critical wavelength λ_{cr}^{cos} :

$$\lambda > \lambda_{cr}^{cos} = 2\pi \sqrt{\frac{R^2 (G\rho C + 2\xi\tau_0)}{-\xi\tau_0}} \approx 2\pi \sqrt{\frac{R^2 G\rho C}{-\xi\tau_0}}$$

For typical values of the shear modulus, the applied shear stress at the boundary, the thermal softening parameter and specific heat, it holds $G\rho C \gg \xi\tau_0$.

6.3 Discussion: rate dependent models versus Cosserat continuum

Even though both frameworks are based on different constitutive assumptions and micro-mechanisms, the resemblance of the expressions for the critical wavelength impels an analogy between the hardening parameter of the viscoplastic model H and the Cosserat internal length, which here is chosen equal to the mean grain radius: $Hc_h \sim R^2 G$. We observe that in the rate-dependent framework, a characteristic length appears from the combination of strain rate hardening and thermal diffusivity, whereas in the Cosserat framework it is directly related to the material grain size. The hardening parameter H can be measured experimentally for a given rock and it generally decreases during shearing together with the size of the grains and the shear modulus, which also decrease due to important shearing and comminution. It is worth mentioning that the term $R^2 G$ represents the

rolling stiffness of the grains, which, in comparison with the classical Cauchy continuum, rigidifies the system in the same way that the viscous term in the rate dependent friction law does. If we take the example of a highly granulated fault gouge with a grain size of $10\ \mu\text{m}$ and assuming a shear modulus $G = 300\ \text{MPa}$, then for $c_{th} = 1\ \text{mm}^2/\text{s}$, the hardening parameter H is equal to $H = 0.03\ \text{MPa s}$, which is in agreement with experimental measurements [68], [69]. Consistently, we observe the similar role of the diffusion length and of the Cosserat internal length in the control of the thickness of the localization zone.

7. Conclusions

In this chapter we summarized the fundamental, balance equations of a Cosserat continuum under multiphysical couplings that involve a fluid and a solid phase. In the beginning the fluid was considered not to react with the solid phase in order to present the basic thermo-hydro-mechanical framework. The additional terms due to fluid momentum, mass and energy exchange were presented next in the case of chemically reactive fluids (thermo-hydro-chemo-mechanical couplings) resulting to phase transitions. Under appropriate, application-wise constitutive laws, the above equations can be used for modeling various physical systems by taking into account the microstructure in a continuum mechanics framework

Cosserat continuum has several advantages. First of all it remedies the mesh dependency of the classical Cauchy continuum and leads to correct energy dissipation in inelasticity and softening. Notice, that the latter is of particular importance in rock mechanics as it controls stress redistribution and failure, in fault mechanics as it determines the seismic energy budget and in soil mechanics especially when non-associative plastic flow behavior is involved. Several examples are presented in section 4. Moreover, Cosserat continuum assures in a physical manner hourglass control in reduced integration finite element formulations.

Finally, a simple example of the adiabatic shearing of a rock layer under constant shear stress is presented in order to highlight the similarities of a rate independent Cosserat and a rate dependent Cauchy continuum as far it concerns strain localization conditions. Cosserat continuum is a promising framework for studying many problems where microstructure is of paramount importance. Faults is one of them [8], [21]–[24].

References

- [1] P. Germain, “The Method of Virtual Power in Continuum Mechanics. Part 2: Microstructure,” *SIAM J. Appl. Math.*, vol. 25, no. 3, pp. 556–575, Nov. 1973.
- [2] D. Besdo, “Ein Beitrag zur nichtlinearen Theorie des Cosserat-Kontinuums,” *Acta Mech.*,

- vol. 20, pp. 105–131, 1974.
- [3] W. B. Anderson and R. S. Lakes, “Size effects due to Cosserat elasticity and surface damage in closed-cell polymethacrylimide foam,” *J. Mater. Sci.*, vol. 29, pp. 3–9, 1994.
- [4] S. Forest, R. Dendievel, and G. R. Canova, “Estimating the overall properties of heterogeneous Cosserat materials,” *Model. Simul. Mater. Sci. Eng.*, vol. 7, no. 5, pp. 829–840, Sep. 1999.
- [5] S. Forest and K. Sab, “Cosserat overall modeling of heterogeneous materials,” *Mech. Res. Commun.*, vol. 25, no. 4, pp. 449–454, Jul. 1998.
- [6] S. Forest, F. Pradel, and K. Sab, “Asymptotic analysis of heterogeneous Cosserat media,” *Int. J. Solids Struct.*, vol. 38, no. 26–27, pp. 4585–4608, Jul. 2001.
- [7] I. Stefanou, J. Sulem, and I. Vardoulakis, “Homogenization of interlocking masonry structures using a generalized differential expansion technique,” *Int. J. Solids Struct.*, vol. 47, no. 11–12, pp. 1522–1536, Jun. 2010.
- [8] J. Sulem, I. Stefanou, and E. Veveakis, “Stability analysis of undrained adiabatic shearing of a rock layer with Cosserat microstructure,” *Granul. Matter*, vol. 13, no. 3, pp. 261–268, Feb. 2011.
- [9] P. Trovalusci, M. Ostoja-Starzewski, M. L. De Bellis, and A. Murrari, “Scale-dependent homogenization of random composites as micropolar continua,” *Eur. J. Mech. - A/Solids*, vol. 49, pp. 396–407, Jan. 2015.
- [10] R. Masiani and P. Trovalusci, “Cosserat and Cauchy materials as continuum models of brick masonry,” *Meccanica*, vol. 31, no. 4, pp. 421–432, Aug. 1996.
- [11] H. B. Mühlhaus and I. Vardoulakis, “The thickness of shear bands in granular materials,” *Géotechnique*, vol. 38, no. 3, pp. 331–331, 1988.
- [12] J. P. Bardet and I. Vardoulakis, “The asymmetry of stress in granular media,” *Int. J. Solids Struct.*, vol. 38, no. 2, pp. 353–367, Jan. 2001.
- [13] E. Pasternak, A. V. Dyskin, and H. B. Mühlhaus, “Cracks of higher modes in Cosserat continua,” *Int. J. Fract.*, vol. 140, no. 1, pp. 189–199, 2006.
- [14] E. Pasternak, A. V. Dyskin, and Y. Estrin, “Deformations in Transform Faults with Rotating Crustal Blocks,” *Pure Appl. Geophys.*, vol. 163, no. 9, pp. 2011–2030, Sep. 2006.
- [15] P. de Buhan and B. Sudret, “Micropolar multiphase model for materials reinforced by linear inclusions,” *Eur. J. Mech. - A/Solids*, vol. 19, no. 4, pp. 669–687, Jul. 2000.
- [16] A. Zervos, P. Papanastasiou, and I. Vardoulakis, “Modelling of localisation and scale effect in thick-walled cylinders with gradient elastoplasticity,” *Int. J. Solids Struct.*, vol. 38, no. 30–31, pp. 5081–5095, Jul. 2001.
- [17] P. Papanastasiou and A. Zervos, “Wellbore Stability Analysis: From Linear Elasticity to Postbifurcation Modeling,” *Int. J. Geomech.*, vol. 4, no. 1, pp. 2–12, Mar. 2004.
- [18] P. C. Papanastasiou and I. Vardoulakis, “Numerical treatment of progressive localization in relation to borehole stability,” *Int. J. Numer. Anal. Methods Geomech.*, vol. 16, no. 6, pp. 389–424, Jun. 1992.
- [19] R. De Borst and L. J. Sluys, “Localisation in a Cosserat continuum under static and dynamic loading conditions,” vol. 90, pp. 805–827, 1991.
- [20] M. Godio, I. Stefanou, K. Sab, and J. Sulem, “Multisurface plasticity for Cosserat materials: Plate element implementation and validation,” *Int. J. Numer. Methods Eng.*, vol. 108, no. 5, pp. 456–484, Nov. 2016.

- [21] H. Rattetz, I. Stefanou, J. Sulem, E. Veveakis, and T. Poulet, "Insight into the different couplings involved in the weakening of faults and their effect on earthquake nucleation," in *American Geophysical Union Fall Meeting*, 2016.
- [22] H. Rattetz, I. Stefanou, and J. Sulem, "Thermo-hydro mechanical couplings and strain localisation in 3D continua with microstructure . Part I : Theory and linear stability analysis," *under Prep.*, 2016.
- [23] E. Veveakis, I. Stefanou, and J. Sulem, "Failure in shear bands for granular materials: thermo-hydro-chemo-mechanical effects," *Géotechnique Lett.*, vol. 3, no. April-June, pp. 31–36, May 2013.
- [24] J. Sulem and I. Stefanou, "Thermal and chemical effects in shear and compaction bands," *Geomech. Energy Environ.*, Feb. 2016.
- [25] R. D. Mindlin, "Micro-structure in linear elasticity," *Arch. Ration. Mech. Anal.*, vol. 16, no. 1, 1964.
- [26] A.-C. Eringen, *Microcontinuum Field Theories*. Springer Verlag, 1999.
- [27] I. Stefanou, J. Sulem, and I. Vardoulakis, "Three-dimensional Cosserat homogenization of masonry structures: elasticity," *Acta Geotech.*, vol. 3, no. 1, pp. 71–83, Feb. 2008.
- [28] G. T. Houlsby and a. M. Puzrin, "A thermomechanical framework for constitutive models for rate-independent dissipative materials," *Int. J. Plast.*, vol. 16, no. 9, pp. 1017–1047, Aug. 2000.
- [29] O. Coussy, *Poromechanics*. Wiley, 2004.
- [30] J. Sulem and I. Stefanou, "Thermal and chemical effects in shear and compaction bands," 2015.
- [31] J. Sulem and V. Famin, "Thermal decomposition of carbonates in fault zones: Slip-weakening and temperature-limiting effects," *J. Geophys. Res.*, vol. 114, no. B3, p. B03309, Mar. 2009.
- [32] N. Brantut, J. Sulem, and A. Schubnel, "Effect of dehydration reactions on earthquake nucleation: Stable sliding, slow transients, and unstable slip," *J. Geophys. Res. Solid Earth*, vol. 116, no. July 2010, pp. 1–16, 2011.
- [33] I. Vardoulakis, *Lecture notes on Cosserat continuum mechanics with application to the mechanics of granular media*, no. January. 2009.
- [34] J. Sulem and I. Vardoulakis, "Bifurcation analysis of the triaxial test on rock specimens. A theoretical model for shape and size effect," *Acta Mech.*, vol. 83, no. 3–4, pp. 195–212, Sep. 1990.
- [35] J. Sulem and I. Vardoulakis, "Bifurcation analysis of the triaxial test on rock specimens. A theoretical model for shape and size effect," *Acta Mech.*, vol. 83, no. 3–4, pp. 195–212, Sep. 1990.
- [36] I. Vardoulakis and J. Sulem, *Bifurcation Analysis in Geomechanics*. Glasgow: Blackie, 1995.
- [37] H.-B. Mühlhaus and I. Vardoulakis, "The thickness of shear bands in granular materials," *Géotechnique*, vol. 37, no. 3, pp. 271–283, Jan. 1987.
- [38] H. B. Mühlhaus and I. Vardoulakis, "The thickness of shear bands in granular materials," *Géotechnique*, vol. 37, no. 3, pp. 271–283, Jan. 1987.
- [39] E. Veveakis, J. Sulem, and I. Stefanou, "Modeling of fault gouges with Cosserat Continuum Mechanics: Influence of thermal pressurization and chemical decomposition as coseismic weakening mechanisms," *J. Struct. Geol.*, vol. 38, pp. 254–264, May 2012.

- [40] R. De Borst, L. J. Sluys, H. B. Mühlhaus, and J. Pamin, “Fundamental issues in finite element analyses of localization of deformation,” *Eng. Comput.*, vol. 10, no. 2, pp. 99–121, Feb. 1993.
- [41] R. De Borst, “Possibilities and limitations of finite elements for limit analysis,” no. 2, pp. 199–210, 1984.
- [42] R. De Borst, “SIMULATION OF STRAIN LOCALIZATION: A REAPPRAISAL OF THE COSSERAT CONTINUUM,” *Eng. Comput.*, vol. 8, no. 4, pp. 317–332, 1991.
- [43] M. Godio, I. Stefanou, K. Sab, and J. Sulem, “Dynamic finite element formulation for Cosserat elastic plates,” *Int. J. Numer. Methods Eng.*, vol. 101, no. 13, pp. 992–1018, Mar. 2015.
- [44] R. E. Goodman, “Introduction to Rock Mechanics.” John Wiley & Sons, Inc., pp. 293–334, 1989.
- [45] K. Mam and S. Quennehen, “Réactivation de faille par géothermie profonde Implémentation d’une loi de frottement sous ABAQUS,” Ecole des Ponts ParisTech, 2016.
- [46] I. Stefanou and S. Alevizos, “Fundamentals of bifurcation theory and stability analysis,” in *Modelling of instabilities and bifurcation in Geomechanics, ALERT geomaterials Doctoral School 2016*, J. Sulem, I. Stefanou, E. Papamichos, and E. Veveakis, Eds. Aussois, France, 2016.
- [47] C. H. Scholz, *The mechanics of earthquakes and faulting*, Second. Cambridge, 2002.
- [48] H. Kanamori and E. E. Brodsky, “The physics of earthquakes,” *Reports Prog. Phys.*, vol. 67, no. 8, pp. 1429–1496, Aug. 2004.
- [49] O. C. Zienkiewicz, R. L. Taylor, and J. M. Too, “Reduced integration technique in general analysis of plates and shells,” *Int. J. Numer. Methods Eng.*, vol. 3, no. 2, pp. 275–290, Apr. 1971.
- [50] O. C. Zienkiewicz, R. L. Taylor, and J. Z. Zhu, *The Finite Element Method*. 2013.
- [51] E. Sánchez-Palencia, “Homogenization in mechanics. A survey of solved and open problems,” *Rend. Sem. Mat. Univ. ...*, vol. 44, pp. 1–46, 1986.
- [52] N. Bakhvalov and G. Panasenko, “Homogenisation: Averaging Processes in Periodic Media: Mathematical Problems in the Mechanics of Composite Materials.” Springer, 1989.
- [53] J. Pinho-da-Cruz, J. a. Oliveira, and F. Teixeira-Dias, “Asymptotic homogenisation in linear elasticity. Part I: Mathematical formulation and finite element modelling,” *Comput. Mater. Sci.*, vol. 45, no. 4, pp. 1073–1080, Jun. 2009.
- [54] N. Charalambakis, “Homogenization Techniques and Micromechanics. A Survey and Perspectives,” *Appl. Mech. Rev.*, vol. 63, no. 3, p. 30803, 2010.
- [55] F. Pradel and K. Sab, “Cosserat modelling of elastic periodic lattice structures,” *Comptes Rendus l’Académie des Sci. ...*, pp. 699–704, 1998.
- [56] K. Sab and F. Pradel, “Homogenisation of periodic Cosserat media,” *Int. J. Comput. Appl. Technol.*, vol. 34, no. 1, p. 60, 2009.
- [57] R. Rezakhani and G. Cusatis, “Asymptotic expansion homogenization of discrete fine-scale models with rotational degrees of freedom for the simulation of quasi-brittle materials,” *J. Mech. Phys. Solids*, vol. 88, pp. 320–345, 2016.
- [58] M. Godio, I. Stefanou, K. Sab, J. Sulem, and S. Sakji, “A limit analysis approach based on Cosserat continuum for the evaluation of the homogenized inplane strength of discrete media,” *Submitt. Publ.*, 2016.

- [59] A. Bacigalupo and L. Gambarotta, "Multi-scale modelling of periodic masonry: characteristic lengths and dispersive waves."
- [60] A. Bacigalupo and L. Gambarotta, "Computational two-scale homogenization of periodic masonry: Characteristic lengths and dispersive waves," *Comput. Methods Appl. Mech. Eng.*, vol. 213–216, pp. 16–28, Mar. 2012.
- [61] D. Baraldi, S. Bullo, and A. Cecchi, "Continuous and discrete strategies for the modal analysis of regular masonry," *Int. J. Solids Struct.*, vol. 84, pp. 82–98, May 2016.
- [62] I. Stefanou and J. Sulem, "Existence of a threshold for brittle grains crushing strength: two-versus three-parameter Weibull distribution fitting," *Granul. Matter*, vol. 18, no. 2, p. 14, May 2016.
- [63] I. Stefanou and J. Sulem, "Chemically induced compaction bands: Triggering conditions and band thickness," *J. Geophys. Res. Solid Earth*, vol. 119, no. 2, pp. 880–899, Feb. 2014.
- [64] M. Godio, I. Stefanou, K. Sab, and J. Sulem, "Cosserat Elastoplastic Finite Elements for Masonry Structures," *Key Eng. Mater.*, vol. 624, pp. 131–138, 2014.
- [65] J. P. Bardet and I. Vardoulakis, "Reply to discussion by Dr . Katalin Bagi," *Int. J. Solids Struct.*, vol. 40, pp. 7683–7683, 2003.
- [66] W. M. Wang, L. J. Sluys, and R. De Borst, "Interaction between material length scale and imperfection size for localisation phenomena in viscoplastic media," *Eur. J. Mech. - A/Solids*, vol. 15, no. 3, pp. 447–464, 1996.
- [67] J. R. Rice, J. W. Rudnicki, and J. D. Platt, "Stability and localization of rapid shear in fluid-saturated fault gouge: 1. Linearized stability analysis," *J. Geophys. Res. Solid Earth*, vol. 119, no. 5, pp. 4311–4333, May 2014.
- [68] M. L. Blanpied, D. A. Lockner, and J. D. Byerlee, "Frictional slip of granite at hydrothermal conditions," *J. Geophys. Res.*, vol. 100, no. B7, p. 13045, 1995.
- [69] F. M. Chester and N. G. Higgs, "Multimechanism friction constitutive model for ultrafine quartz gouge at hypocentral conditions," *J. Geophys. Res.*, vol. 97, no. B2, p. 1859, 1992.